Fibers and Polymers (2023) 24:1681–1693
https://doi.org/10.1007/s12221-023-00165-0

Online ISSN 1875-0052
Print ISSN 1229-9197

REGULAR ARTICLE

Dyeing of Recycled Electrospun Polyamide 6 Nanofibers: Implications of Dye Particle Size

Bahaa S. Metwally[1] · Samah A. Rashed[2] · M. N. El-Sheikh[3] · Asmaa S. Hamouda[4]

Received: 9 December 2022 / Revised: 17 January 2023 / Accepted: 4 March 2023 / Published online: 29 March 2023

Abstract

The dyeing of recycled polyamide nonwoven fabrics based on nanofibers (PA-NWNF), which were fabricated from polyamide wastes, was conducted in this study. Since PA-NWNF exhibited a high surface area to volume ratio, it was dyed with different particle sizes of Disperse Red 167 dye (DR 167, DR 167-B, and DR 167-C) without auxiliary agents to prevent further environmental pollution. The undyed and dyed PA-NWNF, as well as the applied dyes, were characterized by SEM, BET, XRD, and FT-IR techniques. Both color yield (*K/S*) and fastness of dyed PA-NWNF were also evaluated. The morphology of dyed DR 167-C owned homogeneity and smooth nanofibers. In addition, DR 167-C dye (the smallest particle size) provided numerous advantages, including high particle dispersion, low dyeing temperature, minimum processing time, and greater color yield. At a concentration of 15%, DR 167-C produced 55.1 and 33.18% color yields which were higher than DR 167 and DR 167-B, respectively. Also, DR 167-C achieved a better colorfastness to washing (very good, 4) compared to other studied dyes.

Keywords Polyamide nanofiber · Particle size · Dyeing · Recycling · Disperse dye · Nonwoven fabrics

1 Introduction

Nonwoven fabrics based on nanofibers (NWNF) are gaining popularity due to their unique and special properties in terms of waterproofing and vapor permeability with improved breathability [1–3]. Electrospinning has been recognized as the simplest, low-cost, most effective, and versatile technique used to produce NWNF without the need for a weaving process due to its superior cohesiveness [4–10]. NWNF and its modifications are advantageous for several fields, such as biomedical [9, 11, 12], environment [13–16], electronics [17], energy [18], and textile manufacturing [19–27]. Besides the functional properties of NWNF, its esthetic characteristics are also widely considered by industries. The dyeing of NWNF is an integral part of innovative apparel textiles because the dyeing improves its aesthetic property [28], which increases the demand on potential applications of dyed NWNF [3]. The dyeing process of NWNF takes the same line as conventional textiles. Recently, numerous researchers have been endeavoring to improve the dyeability and enhance the aesthetic properties of NWNF. Li et al. modified polyacrylonitrile PAN using the free radical polymerization process to enhance its dyeability with reactive dyestuff [29]. Another study was carried out by Mehdi et al. on dyeing recycled polyethylene terephthalate nanofibers with disperse dyes using dope process [30]. Also, batchwise method for dyeing of electrospun Nylon 6 nanofibers with disperse dyes under ultrasonic energy was investigated by Jatoi et al. [31]. Electron beam irradiation technology was used by Park et al. to the dyeing of electrospun nylon 6 with reactive dyes [32]. Lee et al. applied a high molecular mass acid dyes for nylon 66 nanofiber dyeing [33]. On the other hand, Ahmed et al. used a different types of dyes such as reactive, vat, and disperse dyes on polyamide

✉ Bahaa S. Metwally
Bahaa.saleh14@techedu.bsu.edu.eg

✉ Asmaa S. Hamouda
asmaa_hamouda@psas.bsu.edu.eg

[1] Textile Technology Department, Faculty of Technology and Education, Beni-Suef University, Beni-Suef, Egypt

[2] Textile Printing, Dyeing, and Finishing Department, Faculty of Applied Arts, Beni-Suef University, Beni-Suef, Egypt

[3] Production Technolgy Department, Faculty of Technology and Education, Beni-Suef University, Beni-Suef, Egypt

[4] Head of Environmental Sciences and Industrial Development Department. Faculty of Postgraduate Studies for Advanced Sciences, Beni-Suef University, Beni-Suef, Egypt

[34]. Despite that, the color yield improvement of NWNF remains a significant challenge because of its higher surface area than conventional textiles. As a result, large amounts of dye are required to achieve an acceptable shade depth of dyed NWNF [35, 36]. So, the smallest dye particles with a high surface area may be the key to enhancing nanofiber dyeing quality [37].

Polyamides are semi-crystalline materials with excellent chemical resistance and outstanding mechanical and thermal characteristics [38]. Due to the mass production of polyamides, enormous amounts of their waste are produced annually by textile factories, causing severe environmental problems [39]. Electrospinning offers the opportunity to recycle polyamide wastes to fabricate NWNF based on nanofiber (PA-NWNF) [38, 39]. Disperse dyes are one of the dyes utilized for dyeing polyamides [31]. As a result of the low dispersibility of disperse dye in dyebaths, a specific quantity of dispersing agents has been involved in the disperse dye composition. As a result, a certain amount of dispersing agents and auxiliaries must be used in the dyeing process [40]. Thus, the dyeing effluents have hazardous and toxic impacts on the environmental system [41, 42]. Based on the previous works, the milled disperse dye at different particle sizes has not yet been applied for recycled PA-NWNF dyeing without auxiliaries. Hence, this study aims to dye PA-NWNF with different particle sizes of Disperse Red 167 (DR 167) for apparel uses. The PA-NWNF was recycled from PA 6 wastes using the electrospinning technique. The dyeing parameters such as dye concentration, temperature, and contact time were studied. The undyed and dyed NWNF properties like surface morphology, chemical structure, and crystallinity were evaluated using scanning electron microscopy (SEM), Brunauer–Emmett–Teller (BET), X-ray diffraction (XRD), and Fourier transform infrared spectroscopy (FTIR). Additionally, the color yield and color fastness (washing, perspiration, and light) were evaluated.

2 Experimental

2.1 Materials

Disperse Red 167 (DR167) dye was supplied by DyStar (Cairo, Egypt) and its structure is shown in Fig. 1. PA 6 100% knitted fabric wastes (135 g/m^2) were collected from Salamtex Company, Cairo, Egypt. PA 6 wastes were scoured in a solution containing 1 g/L nonionic detergent for 20 min at 80 °C

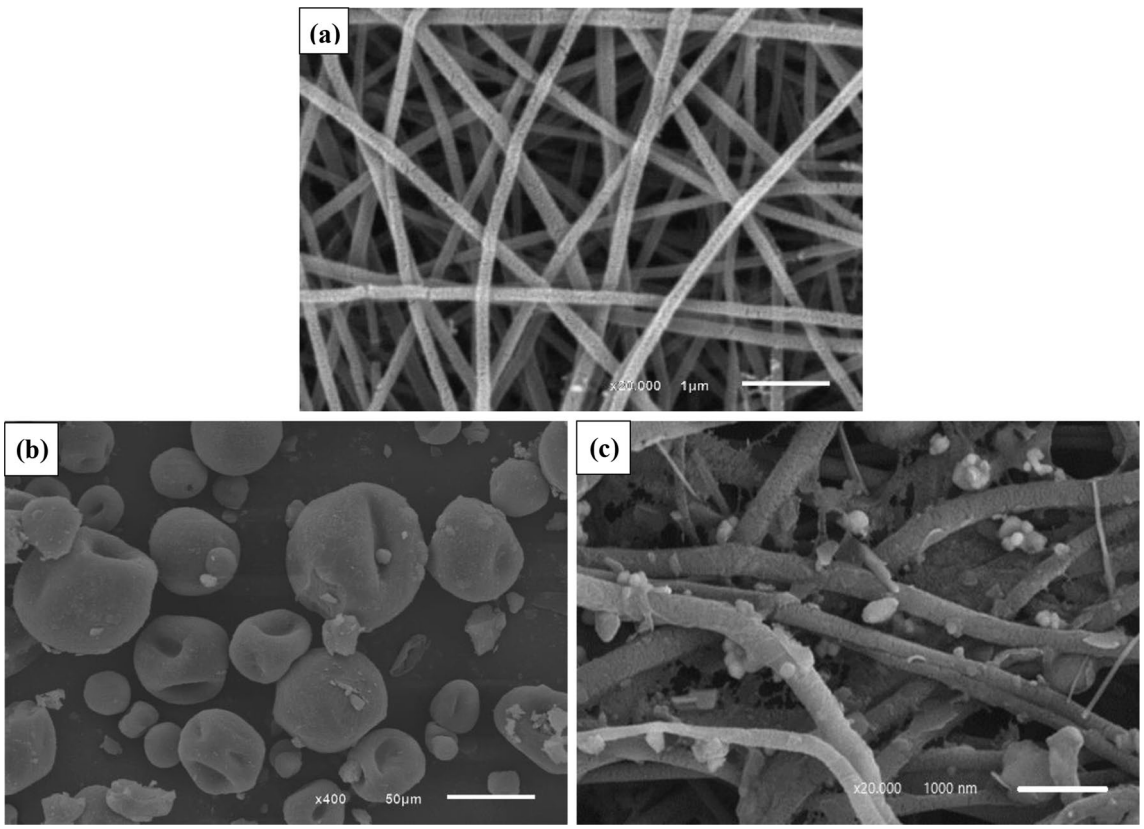

Fig. 1 SEM images of **a** PA-NWNF, **b** DR 167, **c** dyed DR 167

to remove impurities and waxes, and then rinsed thoroughly with cold tap water, and air-dried [39]. Formic acid 90% was supplied by BDH Chemicals (England). Hydrochloric acid and sodium hydroxide were provided by Biochim (Cairo, Egypt).

2.2 Fabrication of PA-NWNF

Based on our experimental work (data not shown), polyamide fabric wastes were dissolved in formic acid at a concentration of 21% wt/wt. The mixture was continuously stirred using a magnetic stirrer at 650 rpm until homogeneous mixing was achieved at room temperature (25 ± 3 °C) A 10 ml plastic syringe with a metallic needle was used for the electrospinning process. With an operating voltage of 20 kV, the positive electrode was connected to the syringe needle, while the negative electrode was attached to the metallic collector to fabricate the PA-NWNF. The distance between the needle tip and the collector was set at 25 cm and the solution flow rate was adjusted to 0.5 ml/h using a programmable syringe pump (NE-4000, USA).

2.3 Dye Preparation

The different particle sizes of DR 167 dye were prepared by intermittent milling, which included short periods of milling lasting 30 min followed by rest intervals lasting 15 min, using a ball mill machine (Planetary Ball Mill PM 100, RETSCH, Germany). Prior to the milling process, the dye undergoes a drying procedure for a duration of 15 min, at a temperature of 60 °C, with the aim of eliminating any remaining moisture content that could lead to an increase in particle aggregation and a decline in the quality of the dye. A total of 200 g of DR 167 was placed in a 500 mL stainless steel jar, along with 7 balls (2 cm in diameter) and 40 balls (0.5 cm in diameter). The jar was subjected to intermittent milling at a fixed rotational speed of 450 RPM, until a total milling time of 2 h was achieved. Following this, the milled dye was passed through a sieve with a mesh size of 38 µm, resulting in the collection of particles larger than 38 µm, which were labeled as DR 167-B. The remaining particles, with sizes smaller than 38 µm, underwent an additional 8 hours of milling to produce a new sample, designated as DR 167-C.

2.4 Dyeing Process

The dyeing of PA-NWNF samples was carried out with DR 167, DR 167-B, and DR 167-C using distilled water. Five dye concentrations (3, 5, 10, 15, and 20% o.w.f) of the dyes mentioned above were prepared with a liquor ratio of 1:500. To optimize the dyeing conditions, the dyeing was carried out at different temperatures (i.e., RT, 60, 80, 100, and 120 °C) for various dyeing times (i.e., 15, 30, 60, 90, and 120 min) at pH 6. After hot rinsing and air drying, the samples were prepared for color yield and fastness properties (i.e., wash, light, and perspiration) measurements.

2.5 Characterization and Measurement

2.5.1 Scanning Electron Microscopy (SEM)

The morphological features of undyed and dyed PA-NWNF, in addition to applied dyes were observed using scanning electron microscopy (SEM, JSM 6700F/JEOL/Tokyo/Japan) with a beam energy of 30 kV and working distance of 11.1–12.2 mm. The SEM images were taken at different magnifications of 400 and 20,000 × for PA-NWNF and dyes, respectively. Before scanning, the samples were splutter coated with gold by a coater device (JEOL-JSM-420, Japan). The images were examined by Image J software to measure the nanofiber diameters [29].

2.5.2 Surface Area Investigations (BET)

The surface areas of both dyes and PA-NWNF (undyed and dyed) were investigated using a Nova Touch LX4 equipment (BET, Quantachrome, USA). Applying the BET approach, N_2 adsorption/desorption tests evaluated the surface area at 77.35 K. The Brunauer–Emmett–Teller equation was used to determine the S_{BET} [43].

2.5.3 X-ray Diffraction (XRD)

The crystallinity and phase identification of addressed dyes and PA-NWNF before and after dyeing were investigated using an X-ray diffractometer (XRD, PANalytical Empyrean, UK) equipped with a Cu-Ka radiation source ($\lambda = 1.5406$ Å) that was operated using an accelerating voltage of 40 kV and an electrical current of 30 mA in the temperature range of 5–80 °C with a 0.04° detector step size and 5.0 min scanning time.

2.5.4 Fourier Transform Infrared Spectroscopy (FTIR)

The functional groups of the addressed dyes, PA-NWNF, and dyed PA-NWNF were investigated by FTIR in the wavenumber range of 400–4000 cm^{-1} using a Bruker FTIR-2000 spectrometer with spectral resolution of 4 cm^{-1}. The dye samples and KBr (Merck) were mixed in a 1:10 ratio to make a translucent pellet disk utilized to identify the functional groups, whereas PA-NWNF samples

(undyed and dyed) were analyzed using the ATR–FTIR mode.

2.5.5 Color Measurement

The spectrophotometer apparatus (ColorEye, 7000A) was employed to determine the *K/S* values of the dyed PA-NWNF samples. The color yields based on *K/S* data were calculated using the Kubelka–Munk equation [44]:

$$\frac{K}{S} = \frac{(1-R)^2}{2R} \times 10$$

where R represents the reflectance value of PA-NWNF samples at maximum absorption, K indicates to the absorption coefficient, and S denotes the scattering coefficient.

2.5.6 Color Fastness Measurement

Colorfastness to washing, perspiration, and light was evaluated for all-dyed PA-NWNF samples based on standard methods. Colorfastness to washing was carried out using a Launder meter based on AATCC Test Method 61-2013 [45], while AATCC Test Method 15-2013 was used to determine the colorfastness of perspiration [46]. Colorfastness to light was assessed based on AATCC Test Method 16A-1972 [47]. The grayscale reference of color change was employed to evaluate the washing and perspiration fastness, whereas the bluescale reference was used to estimate the light fastness [45].

3 Results and Discussion

3.1 Morphological Characteristics

SEM images of the PA-NWNF morphology before and after dyeing were taken at 20,000×, while those of the applied dyes were taken at 400×(Figs. 1 and 2). The undyed

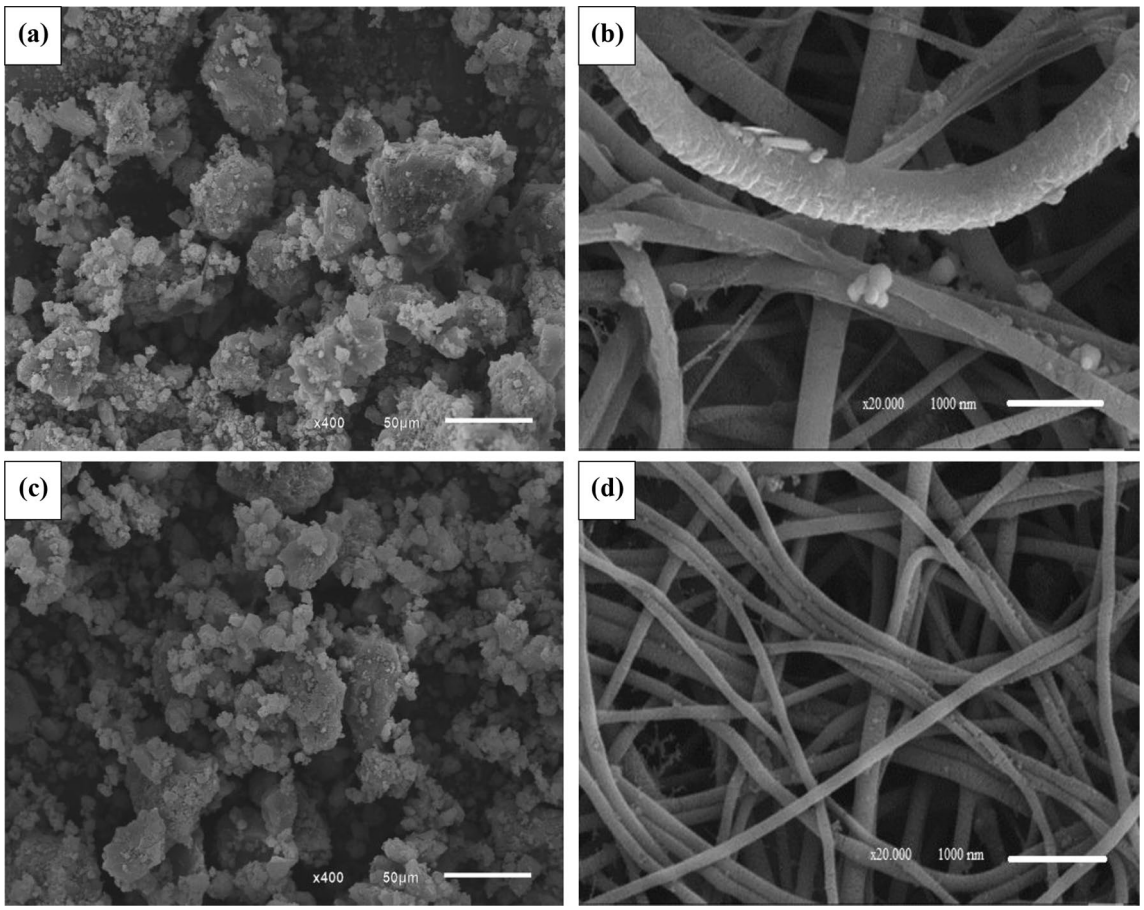

Fig. 2 SEM images of **a** DR 167-B, **b** dyed DR 167-B, **c** DR 167-C and **d** dyed DR 167-C

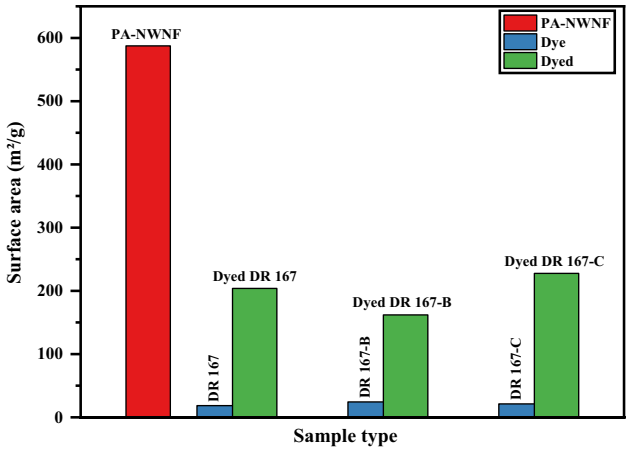

Fig. 3 Surface area of undyed and dyed PA-NWNF and applied dyes

PA-NWNF showed a regular and smooth surface, in addition to the finest homogeneity of fiber diameter with no beads (Fig. 1a). Also, it had a high surface area of about 587.48 m^2/g, as shown in Fig. 3, indicating that the polymer concentration of PA 6 and the employed electrospinning variables were the optimum conditions. The particles of DR 167 and DR 167-B exhibited aggregation on the fiber surface of the dyed PA-NWNF (Figs. 1c and 2b), meanwhile DR 167 (Fig. 1b) showed a higher aggregation in comparison to DR 167-B (Fig. 2a). Such superior aggregation can be correlated with the larger size of DR 167 particles [48]. Moreover, DR 167-B showed a scaly surface of a few fibers which may be due to the aggregation of scale-like particles. Thus, a high reduction in the surface area of the PA-NWNF (161.90 m^2/g) occurred as a result of coating the pores and increasing the fiber diameter of PA-NWNF (Fig. 3). In contrast, the DR 167-C particles (Fig. 2c) became homogenously dispersed and had smaller sizes on the fiber surface (Fig. 2d). This confirms that the enhancement of its dispersion in water is correlated with its smaller particle size [48]. Thus, the dyed DR 167-C has the lowest surface area reduction (227.60 m^2/g), as shown in Fig. 3.

3.2 X-ray Diffraction (XRD)

Usually, PA 6 exhibited two crystalline phases, α (monoclinic, high crystallinity) and γ (pseudo-hexagonal, low crystallinity) [49]. PA 6 molecules undergo hydrogen bonding in both anti-parallel and parallel chain arrangements for the amide groups producing the α- and γ-polymorph phases at $2\theta = 20.3$ and 23.9°, as well as 21.5, respectively [50–54]. XRD spectra of the PA-NWNF and dyed PA-NWNF together with the applied dyes were illustrated in Figs. 4, 5,

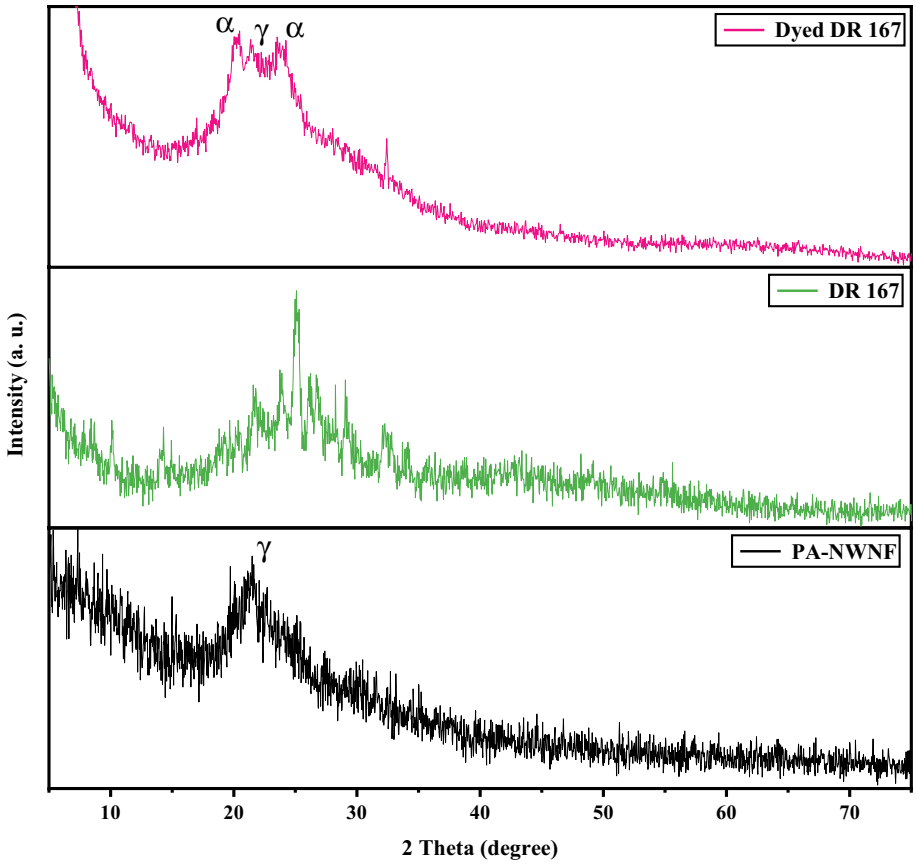

Fig. 4 XRD patterns of PA-NWNF, DR 167 and dyed DR 167

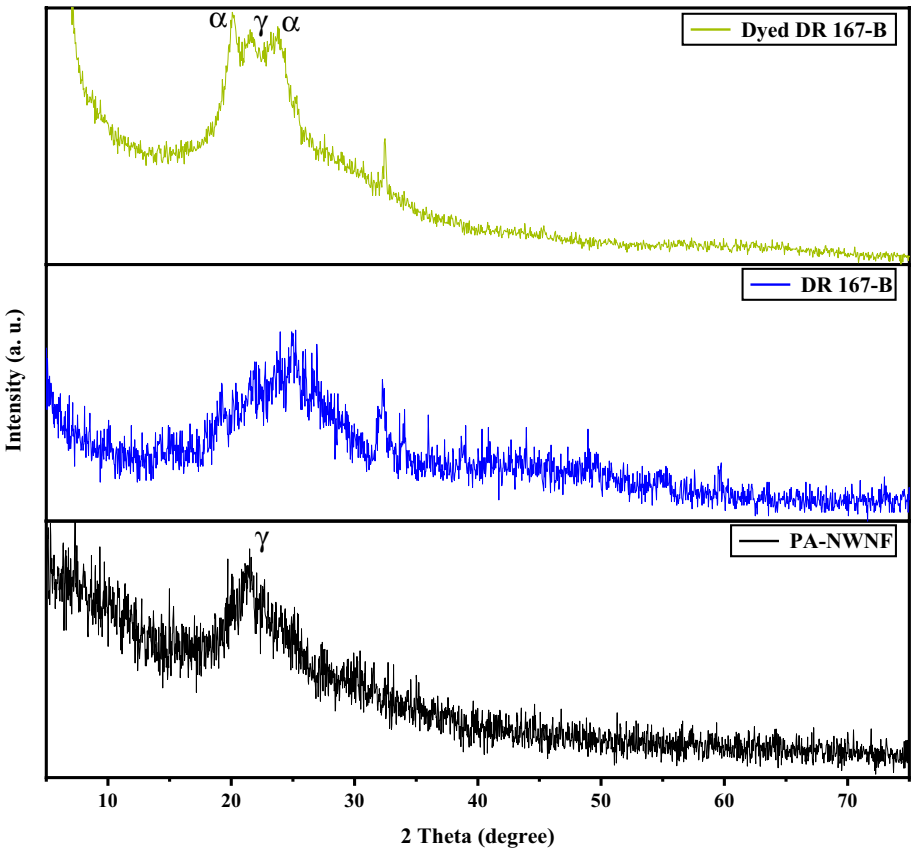

Fig. 5 XRD patterns of PA-NWNF, DR 167-B and dyed DR 167-B

6. The PA-NWNF spectrum had a dominant broader diffraction peak at $2\theta \simeq 21.55°$ with a *d*-spacing value of 4.12 Å, confirming the phase transition of PA 6 to the γ-phase during the electrospinning (Figs. 4, 5, 6) [55]. This is due to the rapid evaporation of solvent during the electrospinning processing of PA 6. Hence, the development of the γ-phase appeared, and the α-phase disappeared [55–58].

After dyeing with DR 167, DR 167-B, and DR 167-C, the complete formation of the α-phase was observed, at $2\theta \simeq 20.27$ and 23.95° with the *d*-spacing value of 4.37 and 3.74 Å, respectively, beside the γ-phase at 21.5° with the *d*-spacing value 4.12 Å (Figs. 4, 5, 6). This can be attributed to the slow heating during the dyeing process, where the existent γ-phase of PA-NWNF melts and then the molecules are recrystallized into α-form (thermodynamically stable) together with γ-form [59–61]. Furthermore, another new diffraction peak at $2\theta \simeq 32.64°$ with a *d*-spacing value of 2.77 Å is inherited from the applied dyes with slight shifting in the distinguishing 2θ (Figs. 4, 5, 6). This was assured by matching peak intensity of dyed PA-NWNF with that of its applied dye (Figs. 4, 5, 6).

3.3 Fourier Transform Infrared Spectroscopy (FTIR)

The effects of dying process on both chemical structures of PA-NWNF and applied dyes were examined by FTIR analysis and illustrated in Figs. 7, 8, 9. As well the functional groups of PA-NWNF were gathered in Table 1. The spectra of PA-NWNF revealed that the absorption bands at 1640.38 and 1543.11 cm^{-1} (amide I and amide II, respectively) are related to the nature of polyamide materials [62], whereas the peaks at 3297.1 and 3087.13 cm^{-1} are correlated to N–H stretching vibration mode (Free and hydrogen bonded N–H stretching, respectively) [63–66]. The asymmetrical and symmetrical stretching, as well as the scissoring vibration of the CH_2 group in the polyamide backbone, can be assigned to the absorption bands at 2931.80, 2860.92 and 1462.71 cm^{-1}, orderly [67, 68]. Furthermore, the vibration of CH_3 groups related to terminal chains and C–N stretching were observed at 1262.33 and 1075.00 cm^{-1}, respectively [69]. Also, the adsorption band of the C=O group overlapped with the band of amide I at 1640.38 cm^{-1} [50, 69]. We can also see the γ-phase of PA-NWNF predominating through recorded bands at 1437.46 cm^{-1} (CH_2 bending vibration) [70–72]. Moreover, twist-wag vibration of the CH_2 group was observed at 1368.48 and 1234.77 cm^{-1} [71, 73]. Also, band at 1168.08 cm^{-1} revealed the bending of the CH_2 group

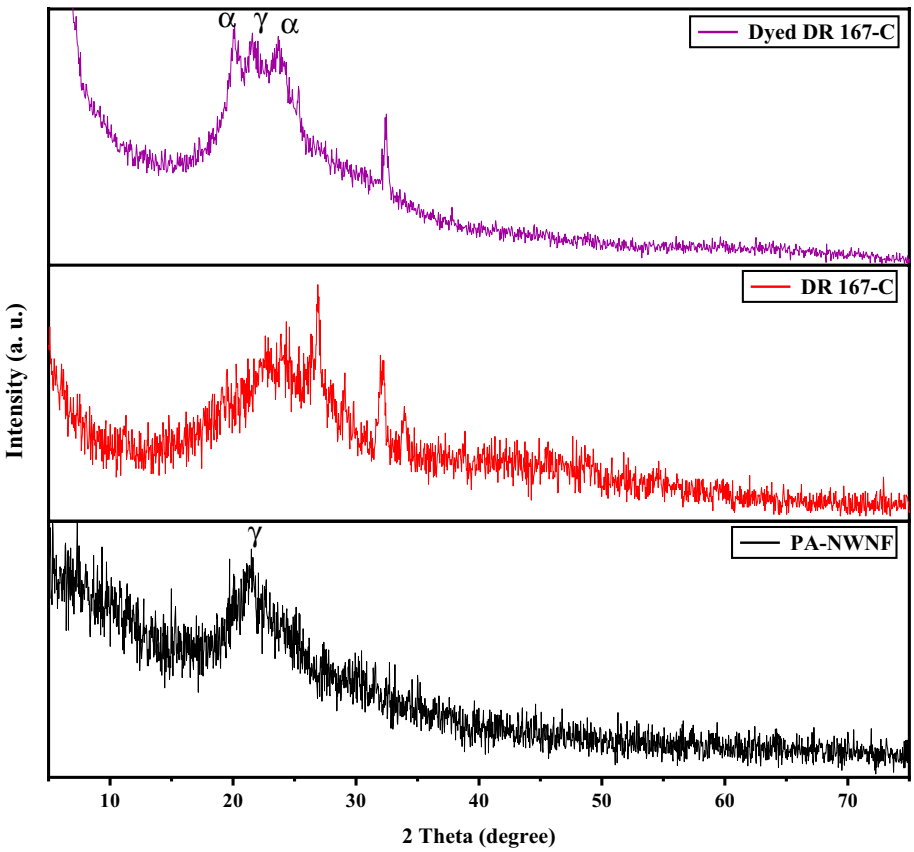

Fig. 6 XRD patterns of PA-NWNF, DR 167-C and dyed DR 167-C

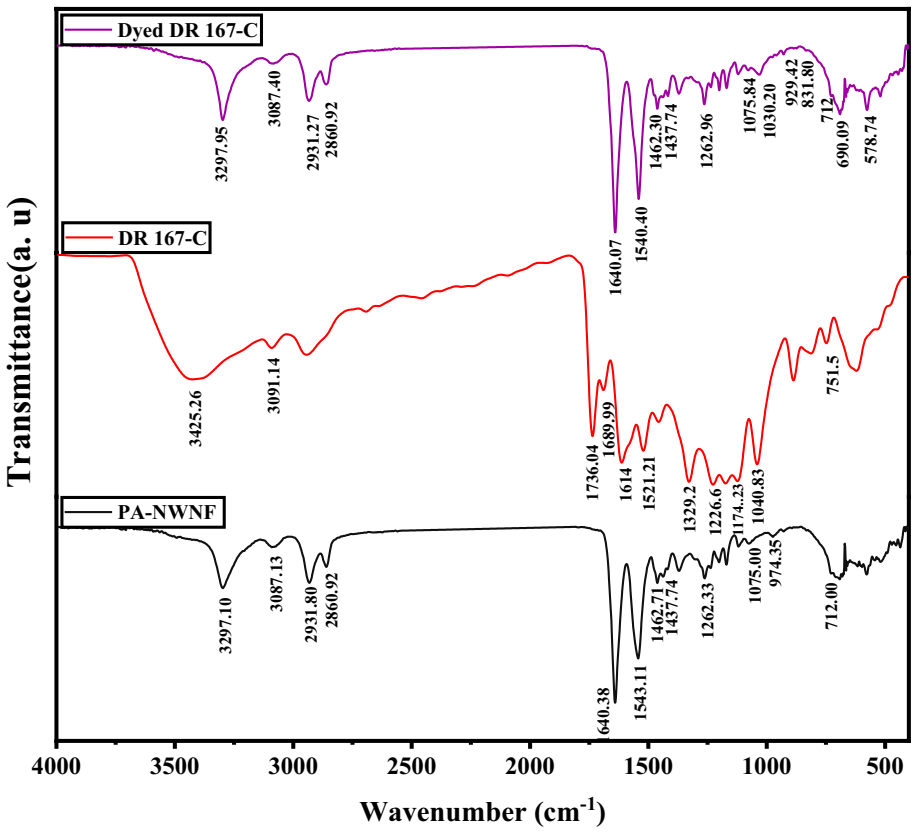

Fig. 7 FTIR spectra of PA-NWNF, DR 167 and dyed DR 167

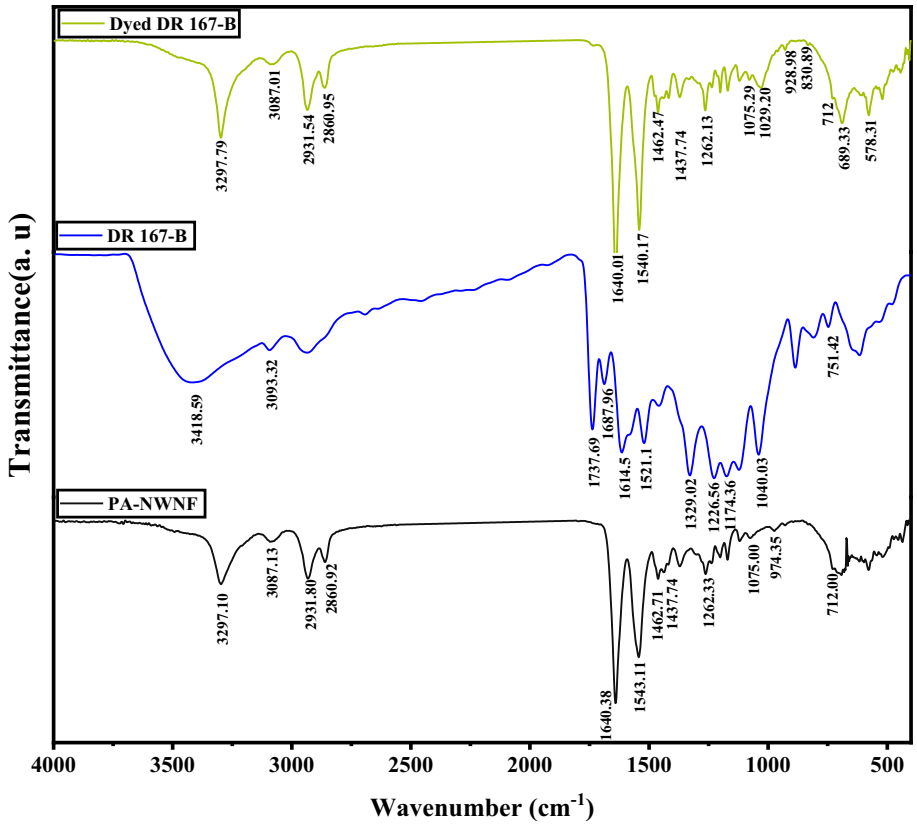

Fig. 8 FTIR spectra of PA-NWNF, DR 167-B and dyed DR 167-B

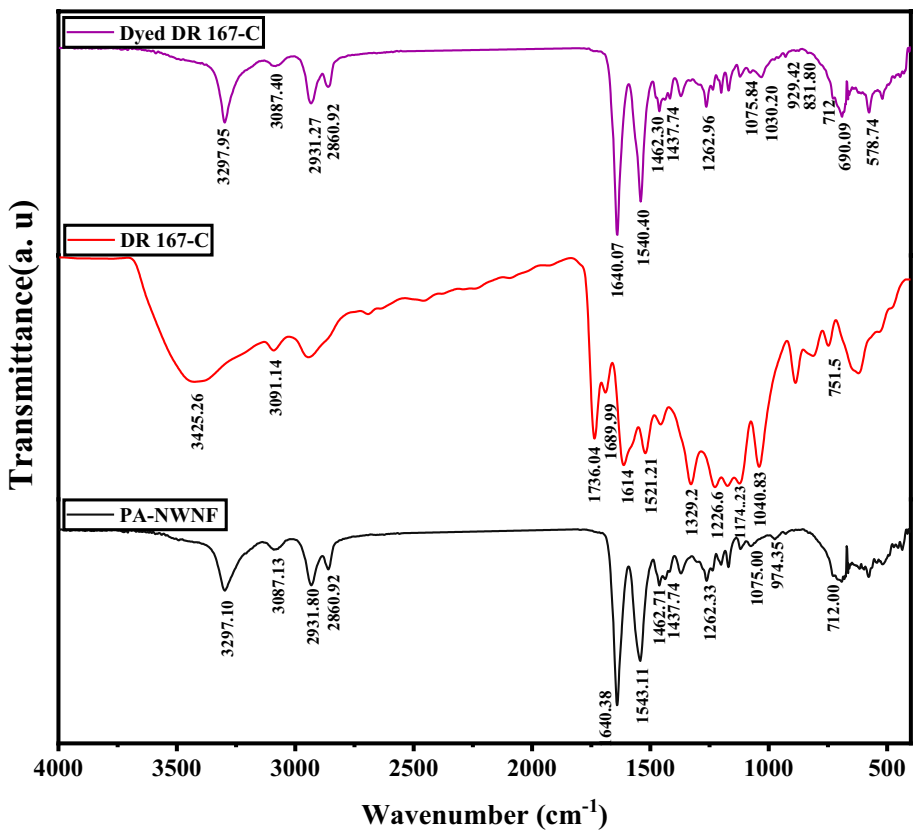

Fig. 9 FTIR spectra of PA-NWNF, DR 167-C and dyed DR 167-C

Table 1 Functional groups of PA-NWNF

Assignments	Wavenumber, cm^{-1}	References
Free N–H and stretching	3297.1	[63–66]
hydrogen bonded (N–H) stretching	3087.13	[63–66]
CH_2 asymmetrical stretching	2931.80	[67, 68]
CH_2 symmetrical stretching	2860.92	[67, 68]
CH_2 scissoring vibration (α-plane)	1476.21	[70, 71, 77, 78]
Amide I, overlapped C=O group	1640.38	[50, 69]
Amide II	1543.11	[62]
CH_2 scissoring vibration	1462.71	[67, 68]
CH_2 bending vibration (γ-plane)	1437.46	[70, 72, 88]
Twist-wag vibration of CH_2 (γ-plane)	1368.48	[71, 73]
CH_3 vibration in terminal chains	1262.33	[69]
Bending of CH_2 (γ-plane)	1168.08	[74, 75]
C–N stretching vibration	1075.00	[69]
CO–NH vibration (α-plane)	1027.20	[50, 62]
CO–NH vibration (γ-plane)	973.90	[62, 71, 73]
CO–NH vibration (α-plane)	958.55	[50, 62]
C–CO stretching vibration (α-plane)	928.86	[70]
CH_2 rocking (α-plane)	831.80	[63]

[74, 75]. The vibration band at 973.90 cm^{-1} is correlated to CO–NH in γ-plane [62, 71, 73]. This is due to the γ-phase transition of PA 6 during the electrospinning process [55, 57, 73, 76]. In contrast, the α-peaks observed in the FTIR results of PA-NWNF reflect the pseudo-crystalline form of α-phase. Figures 7, 8, 9 also showed the FTIR spectra of applied dyes, illustrating differences in the intensities with slight peak shifting, as a function of milling duration. While DR-167 had the β-crystal form, DR 167-B had an overall amorphous nature with initial transformation to the α-crystal form and the complete transformation to the α-crystal form occurred in DR-167-C. After the dyeing process, the PA-NWNF exhibited the two α- and γ-phases. This was corroborated by the emergence of new α peaks at 831.80, 928.86, 958.55, 1027.20, and 1476.21 cm^{-1}, in addition to the presence of γ-phase peaks at 712, 974.21, and 1437.74 cm^{-1} [54, 70, 77–79]. In addition, the bands of amides V and VI were related to α- form at 690.40 and 578.00 cm^{-1}, respectively [56, 80]. Also, it can be observed that the amide II peak shifted from 1543.11 to ≃1540.40 cm^{-1}. The shifting of the amide II peak towards lower frequency indicates the formation of thermodynamically stable α-phase in PA-NWNF [63, 73, 80]. These findings matched with XRD results. The interaction between the dyes and PA-NWNF is not evident in the IR spectra (Figs. 7, 8, 9). This may be due to the small quantities of dyes employed in the experiments, as previously reported in other studies [81–83].

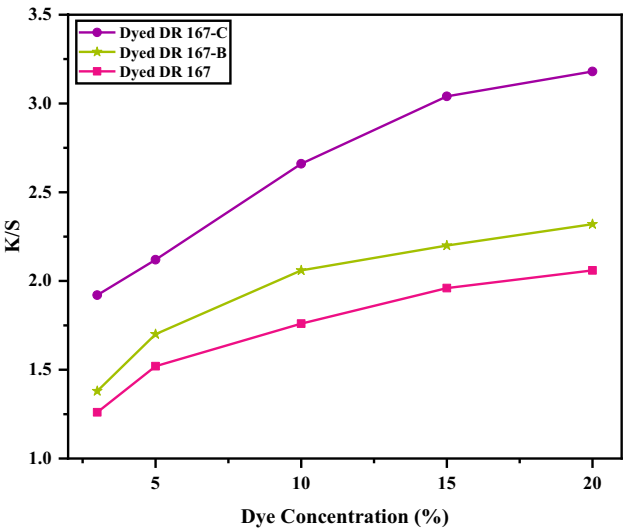

Fig. 10 Effect of dye concentration on color yield

3.4 Effect of Dye Concentration

The effects of dye concentration on color yield were studied at 100 °C for 60 min. Five concentrations (3, 5, 10, 15, and 20% o.w.f) of each dye were utilized and the color yield property was measured in terms of *K/S* values, as shown in Fig. 10. The results showed an increase in the dye concentration corresponding to an increase in *K/S* values for all dyes. Comparing between the *K/S* values of dyed samples, it was found that a 5% concentration of DR 167-C produced color yield almost equal to a 15% concentration of DR 167 and

DR 167-B. In addition, 15% of DR 167-C produced about 55.1 and 33.18% color yield higher than DR 167 and DR 167-B, respectively. This demonstrates that DR 167-C dye exhibited an excellent ability to build color on PA-NWNF. Dyeing synthetic textiles with disperse dyes is generally based on the swelling of the amorphous region in the fiber under high temperature and pressure, which makes adsorbed dye particles on the fiber surface easily penetrate into the fiber inside [42, 84]. Accordingly, dye particles larger than the fiber diameter cannot penetrate into the fiber. Therefore, the difficulty of dyeing nanofibers with disperse dyes is not only because of the high surface area of nanofibers but also the large diameters of the conventional dye particles (average size ≃ 42.2 μm), which are larger than nanofibers diameters. Hence, it cannot penetrate into the fibers and thus be removed with washing. So, the increase in *K/S* of DR 167-C is attributed to the large number of small particles of dye that penetrated into nanofibers. In contrast, the decrease in *K/S* of DR 167 and DR 167-B is attributed to the small number of dye particles much smaller than the nanofiber diameter. This was confirmed by results of the SEM (Figs. 1b and 2a). 15% was chosen as the optimum dye concentration.

3.5 Effect of Dyeing Temperature

To optimize the dyeing temperature, PA-NWNF samples were dyed with 15% dye concentration of each dye for 60 min. Dyeing was carried out at five different temperatures (R.T., 60, 80, 100, and 120 °C). Figure 11 displayed the color yield of dyed PA-NWNF as a function of temperature. The color yield of dyed DR 167-C increased rapidly as the dyeing temperature increased from room temperature to 80 °C, whereas the color yield of dyed DR 167

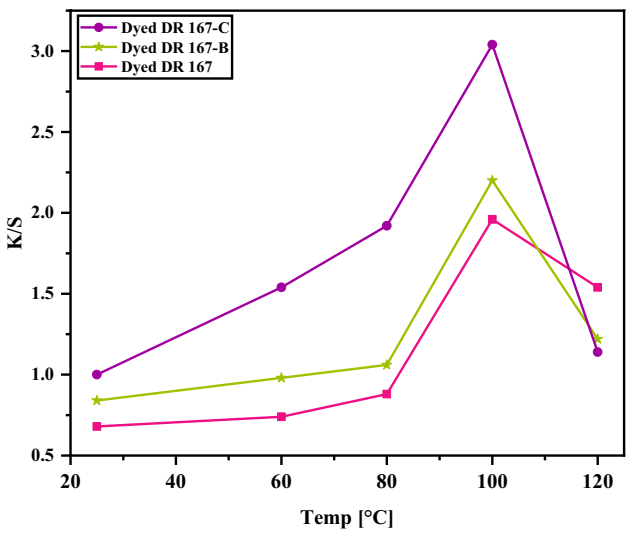

Fig. 11 Effect of dyeing temperature on color yield

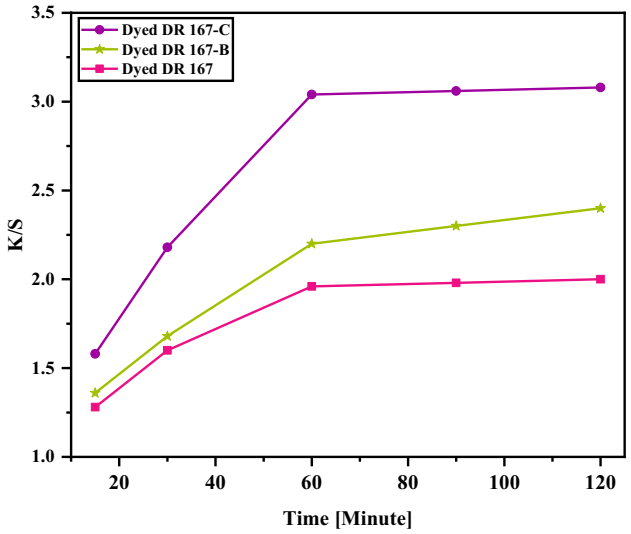

Fig. 12 Effect of dyeing time on color yield

and DR 167-B improved slowly at this temperature rising region. This indicates that particles of DR 167-C dye need low activation energy of diffusion to penetrate the polymer chains compared to the others [85]. From 80 to 100 °C, all dyes showed a steep increase in color yield. This confirms the dye's high dispersion ability in the absence of dyeing auxiliaries, which is consistent with SEM results (Fig. 2d). Furthermore, increasing the dyeing temperature after 100 °C resulted in a decrease in dye substantivity, resulting in a lower color yield [86, 87]. So, the dyeing is optimized at 100 °C.

3.6 Effect of Dyeing Time

To investigate the effects of dyeing time on the color yield of dyed PA-NWNF, the dyeing process was carried out using 15% dye concentration at 100 °C for five different dyeing times (15, 30, 60, 90, and 120 min) as presented in Fig. 12. For all dyes, it was noticed that with increasing the time, the color yield increased and beyond 60 min no further increase in color yield was observed. However, DR 167-C achieved the highest color yield compared to DR 167 and DR 167-B. More specifically, at 60 min, the *K/S* of 3.04 was attained for dyed DR 167-C, while the *K/S* of 2.2 and 1.96 were achieved for dyed DR 167 and DR 167-B, respectively. This was attributed to the rapid movement of small particles of DR 167-C dye, which diffused more quickly into PA-NWNF than the other dyes with larger particle sizes. Thus, the dyeing process was optimized for 60 min.

Table 2 Color fastness of dyed PA-NWNF

Samples	Washing fastness							Perspiration fastness							Light fastness
	Change of shade	Staining on multi-fiber						Change of shade	Staining on multi-fiber						
		CT	CO	PA	PES	PAC	WO		CT	CO	PA	PES	PAC	WO	
Dyed DR 167	3–4	3	4–5	3	4	4–5	4	4–5	3	3–4	3	3–4	3–4	3–4	3
Dyed DR 167-B	3–4	3–4	4–5	3–4	4–5	4–5	4	4–5	3	3–4	3	3–4	3–4	3–4	3
Dyed DR 167-C	4	3–4	4–5	3–4	4–5	5	4	4–5	3	3–4	3	3–4	3–4	3–4	3

Dyeing conditions: dye concentration 15%, temperature 100 ℃, time 60 min, and pH 6

CT cellulose triacetate, *CO* cotton, *PA* polyamide, *PES* polyester, *PAC* polyacrylic, *WO* wool

3.7 Color Fastness Properties

The resistance of dyed fabrics to color bleed against various factors, such as washing, perspiration, and light, is essential. At previously optimized conditions of the dyeing process, the color fastness to washing and perspiration (i.e., shade change and staining), furthermore, the light fastness of dyed PA-NWNF with the addressed dyes were evaluated, as shown in Table 2. The results demonstrated that the color fastness to washing has a very good grade (i.e., shade change) for DR 167-C, while it decreased to a good grade for DR 167-B and DR 167-C. All dyes showed a moderate to excellent range of colorfastness to washing in terms of staining, where staining rates increased for DR 167 and DR 167-B dyes. This finding matched with the data given in Figs. 1 and 2, since the highly dispersed and penetrated particles were obtained in dyed DR 167-C, suggesting that more dye molecules offered high resistance to washing on the test specimen. However, DR 167 and DR 167-B that aggregated on PA-NWNF surface can be easily removed during the test. Moreover, the ratings of perspiration fastness (i.e., shade change and staining) were the same for all dyes. The color change rate was recorded as 4/5, which is an excellent rate. In addition, the color staining on multifiber fabric was rated from moderate to very good. Generally, polyamide and acetate were always found to be the highly stained parts of the multifiber fabrics dyed PA-NWNF. The fastness to light showed the same ratings for all dyes, where overall light fastness had moderate properties.

4 Conclusion

PA-NWNF-based polyamide wastes were electrospun to fabricate very cheap and efficient nonwoven fabric and then dyed using different particle sizes of Disperse Red 167. The dyeing was carried out without auxiliary agents to reduce environmental pollution and dyeing costs. The effects of dye particle size on the morphology and color characteristics were investigated intensively. The dyeing of DR 167-C had advantages over that of DR 167 and DR 167-B. SEM analysis illustrated that PA-NWNF had a regular and smooth surface, in addition to the homogeneity and beadless nanofibers. The smallest particle sizes of DR 167-C dye have a high dispersion in the dyeing process without auxiliary agents, and DR 167-C dye had the lowest effect on the surface area reduction of PA-NWNF, unlike DR 167 and DR 167-B. The XRD and FTIR data confirmed the transformation of the γ-phase of electrospun PA-NWNF into a hybrid dynamically stable α-phase and γ-phase after the dyeing process. The dyeing properties indicated that DR 167-C had a greater affinity of PA-NWNF than other applied dyes. The dyeing conditions were optimized at 15% dye concentration, 60 min, and 100 °C. DR 167-C showed better color yield and colorfastness to washing than DR 167 and DR 167-B. More specifically, DR 167-C produced 55.1 and 33.18% color yields higher than DR 167 and DR 167-B, respectively. Related to colorfastness, all dyed samples showed excellent and moderate fastness to perspiration and light, respectively. The addressed PA-NWNF may be recommended for advanced apparel applications due to its lower energy consumption, cheap materials, and better color yield.

Acknowledgements The authors are gratefully acknowledging the financial support from Beni-Suef University, University performance development center, support and project finance office, project ID YR4-BSU2124.

Author Contributions Conceptualization, methodology, and writing-original draft: BSM; Methodology and writing-review and editing: SAR; Project administration and writing-review and editing: MNE-S; Methodology, writing, review and editing: ASH.

Funding Open access funding provided by The Science, Technology & Innovation Funding Authority (STDF) in cooperation with The Egyptian Knowledge Bank (EKB). The work was supported by the Research Grant for university performance development center, support and project finance office (YR4-BSU2124) from Beni-Suef University, Egypt.

Data availability Data will be made available on request.

Declarations

Conflict of interest The author declares that they have no competing interests.

References

1. L. Van der Schueren, T. Mollet, Ö. Ceylan, K. De Clerck, Eur. Polym. J. **46**, 2229 (2010)
2. Z. Khatri, F. Ahmed, A.K. Jhatial, M.I. Abro, G. Mayakrishnan, I.-S. Kim, Cellulose **21**, 3089 (2014)
3. M. Khatri, U.A. Qureshi, F. Ahmed, Z. Khatri, I.S. Kim, in *Handbook of Nanofibers*. ed. by A. Barhoum, M. Bechelany, A.S.H. Makhlouf (Springer, Berlin, 2018), pp.373–388
4. R. Beigmoradi, A. Samimi, D. Mohebbi-Kalhori, Polymer **143**, 271 (2018)
5. G. Amini, S. Samiee, A.A. Gharehaghaji, F. Hajiani, Adv. Polym. Technol. **35**, 419 (2016)
6. B. Ding, J. Yu, *Electrospun Nanofibers for Energy and Environmental Applications* (Springer, Berlin, 2014)
7. N.R. Dhineshbabu, G. Karunakaran, R. Suriyaprabha, P. Manivasakan, V. Rajendran, Nanomicro. Lett. **6**, 46 (2014)
8. K. Koenig, N. Balakrishnan, S. Hermanns, F. Langensiepen, G. Seide, Materials **13**, 1055 (2020)
9. N.K. Balakrishnan, K. Koenig, G. Seide, Polymers (Basel) **12**, 2321 (2020)
10. S.K.S. Kumar, C. Prakash, Iran Polym. J. **30**, 1263 (2021)
11. S. Agarwal, J.H. Wendorff, A. Greiner, Polymer **49**, 5603 (2008)
12. A. Shiohara, B. Prieto-Simon, N.H. Voelcker, J. Mater. Chem. B **9**, 2129 (2021)
13. S. Borhani, J. Text. Polym. **4**, 45 (2016)
14. P. Brown, C. Cox, *Fibrous Filter Media* (Woodhead Publishing, New York, 2016)
15. A.A. Merati, M.K. Kangazi, in *Environmental Nanotechnology for Water Purification*. ed. by S. Ul-Islam (Wiley, Boca Raton, 2020), p.217
16. V.V. Kadam, L. Wang, R. Padhye, J. Ind. Text. **47**, 2253 (2016)
17. D. Joly, J.-W. Jung, I.-D. Kim, R. Demadrille, J. Mater. Chem. C **4**, 10173 (2016)
18. J. Xue, T. Wu, Y. Dai, Y. Xia, Chem. Rev. **119**, 5298 (2019)
19. J. Hu, *Active Coatings for Smart Textiles*, 1st edn. (Woodhead Publishing, 2016)
20. V.M.M. SaberiMotlagh, O. Emamgholipour, A.K. Haghi, in *Development of Nanotechnology in Textiles*. ed. by A.K. Haghi, G.E. Zaikov (Nova Science, 2012)
21. M. Mirjalili, S. Zohoori, J. Nanostruct. Chem. **6**, 207 (2016)
22. R. Mishra, J. Militky, *Nanotechnology in Textiles: Theory and Application* (Woodhead Publishing, 2018)
23. P. Miśkiewicz, World Sci. News **100**, 74 (2018)
24. H.S. Mohapatra, A. Chatterjee, S. Maity, Int. J. Recent Technol. Eng. **2**, 132 (2013)
25. A.P.S. Sawhney, B. Condon, K.V. Singh, S.S. Pang, G. Li, D. Hui, Text. Res. J. **78**, 731 (2008)
26. T.I. Shaheen, J. Text. Inst. **113**, 2274 (2021)
27. M. Joshi, *Nanotechnology in Textiles: Advances and Developments in Polymer Nanocomposites* (CRC Press, Boca Raton, 2020)
28. F. Ahmed, U.A. Qureshi, Z. Khatri, Mater. Sci. Forum **916**, 10 (2018) https://doi.org/10.4028/www.scientific.net/MSF.916.10
29. X. Li, Y. Yang, H. Zhang, Z. Quan, X. Qin, F. Li, R. Wang, J. Yu, Appl. Nanosci. **10**, 2025 (2020)
30. M. Mehdi, F.K. Mahar, U.A. Qureshi, M. Khatri, Z. Khatri, F. Ahmed, I.S. Kim, Adv. Polym. Technol. **37**, 2820 (2018)
31. A.W. Jatoi, F. Ahmed, M. Khatri, A. Tanwari, Z. Khatri, H. Lee, I.S. Kim, Ultrason. Sonochem. **39**, 34 (2017)
32. M. Park, M.M. Rabbani, H.K. Shin, S.-J. Park, H.Y. Kim, J. Ind. Eng. Chem. **39**, 16 (2016)
33. K.S. Lee, B.S. Lee, Y.H. Park, Y.C. Park, Y.M. Kim, S.H. Jeong, S.D. Kim, Fibers Polym. **6**, 35 (2005)
34. F. Ahmed, U.A. Qureshi, Z. Khatri, Int. J. Chem. Eng. Appl. **10**(1), 1 (2019). https://doi.org/10.18178/ijcea.2019.10.1.730
35. S.M. Burkinshaw, Y.-A. Son, Dyes Pigm. **87**, 132 (2010)
36. S.J. Fang, G.F. Feng, Y.Q. Guo, W.G. Chen, H.F. Qian, Dyes Pigm. **176**, 108225 (2020)
37. Y. Qin, M. Yuan, Y. Hu, Y. Lu, W. Lin, Y. Ma, X. Lin, T. Wang, Int. J. Biol. Macromol. **152**, 280 (2020)
38. M.N. El-Sheikh, B.S. Metwally, M.F. Mubarak, H.A. Ahmed, T. Abdel Moghny, A.M. Zayed, Polym. Bull (2022). https://doi.org/10.1007/s00289-022-04459-w
39. B.S. Metwally, A.A. El-Sayed, E.K. Radwan, A.S. Hamouda, M.N. El-Sheikh, M. Salama, Egypt. J. Chem. **61**, 867 (2018)
40. Y. Qin, D. Yang, X. Qiu, A.C.S. Sustain, Chem. Eng. **3**, 3239 (2015)
41. I. Arslan Alaton, G. Insel, G. Eremektar, F. GermirliBabuna, D. Orhon, Chemosphere **62**, 1549 (2006)
42. L. Pei, Y. Huang, H. Zhang, J. Wang, J. Text. Inst. **113**, 185 (2022)
43. A.M. Zayed, M. Fathy, M. Sillanpää, M.S.M. Abdel Wahed, SN Appl. Sci. **2**, 740 (2020)
44. A. Khatri, S. Ali, A.K. Jhatial, S.H. Kim, Color. Technol. **131**, 374 (2015)
45. F. Saad, A.L. Mohamed, M. Mosaad, H.A. Othman, A.G. Hassabo, Carbohydr. Polym. Technol. **2**, 100132 (2021)
46. B.M. Hegazy, H. Othman, A.G. Hassabo, J. Text. Color. Polym. Sci. **19**, 155 (2022)
47. T. Abou Elmaaty, M. Sofan, S. Ayad, E. Negm, H. Elsisi, J CO2 Util **61**, 102053 (2022)
48. S. Fu, G. Zhang, L. Ding, A. Tian, C. Wang, J. Appl. Polym. Sci. **120**, 3581 (2011)
49. M.V. Jose, B.W. Steinert, V. Thomas, D.R. Dean, M.A. Abdalla, G. Price, G.M. Janowski, Polymer **48**, 1096 (2007)
50. J.C. Farias-Aguilar, M.J. Ramírez-Moreno, L. Téllez-Jurado, H. Balmori-Ramírez, Mater. Lett. **136**, 388 (2014)
51. C. Isbasar, J. Hacaloglu, J. Anal. Appl. Pyrol. **98**, 221 (2012)
52. R. Nirmala, R. Navamathavan, M.H. El-Newehy, H.Y. Kim, Polym. Int. **60**, 1475 (2011)
53. C. Ramesh, E.B. Gowd, Macromolecules **34**, 3308 (2001)
54. R. Dai, M. Huang, L. Ma, W. Liu, S. He, H. Liu, C. Zhu, Y. Wang, Z. Zhang, A. Sun, Adv. Compos. Hybrid Mater. **3**, 522 (2020)
55. J.S. Stephens, D.B. Chase, J.F. Rabolt, Macromolecules **37**, 877 (2004)
56. M. Zoccola, A. Montarsolo, A. Aluigi, A. Varesano, C. Vineis, C. Tonin, E-Polym. **7**, 1204 (2007)
57. P. Heikkilä, A. Taipale, M. Lehtimäki, A. Harlin, Polym. Eng. Sci. **48**, 1168 (2008)

58. M. Sohrabi, M. Razbin, M. Pourtavvaf, R. Bagherzadeh, M. MehdipourMirmahale, J. Text. Inst. (2022). https://doi.org/10.1080/00405000.2022.2145440
59. Y. Liu, L. Cui, F. Guan, Y. Gao, N.E. Hedin, L. Zhu, H. Fong, Macromolecules **40**, 6283 (2007)
60. S.Y. Tsou, H.S. Lin, C. Wang, Polymer **52**, 3127 (2011)
61. A. Abdal-hay, H.M. Mousa, A. Khan, P. Vanegas, J.H. Lim, Colloid Surf. A **457**, 275 (2014)
62. K.H. Lee, K.W. Kim, A. Pesapane, H.Y. Kim, J.F. Rabolt, Macromolecules **41**, 1494 (2008)
63. R. Gupta, K. Pancholi, R. De Sa, D. Murray, D.H. Huo, G. Droubi, M. White, J. Njuguna, JOM **71**, 3119 (2019)
64. I. Hanno, C. Anselmi, K. Bouchemal, Pharm. Res. **29**, 559 (2012)
65. N. Du, C.-Y. Zhao, Q. Chen, G. Wu, R. Lu, Mater. Chem. Phys. **120**, 167 (2010)
66. K. Liu, Y. Li, L. Tao, R. Xiao, RSC Adv. **8**, 9261 (2018)
67. S.K. Bhullar, D. Rana, B.K. Ozsel, M. Orhan, M.B.G. Jun, H.S. Buttar, S. Ostrovidov, M. Ramalingam, J. Nanosci. Nanotechnol. **18**, 2951 (2018)
68. J. Wan, Z.-Y. Bu, C. Li, H. Fan, B.-G. Li, Thermochim. Acta **524**, 117 (2011)
69. I. Ebrahimi, M.P. Gashti, Color. Technol. **132**, 162 (2016)
70. M. Porubská, O. Szöllős, A. Kóňová, I. Janigová, M. Jašková, K. Jomová, I. Chodák, Polym. Degrad. Stabil. **97**, 523 (2012)
71. Q.J. Wu, X.H. Liu, L.A. Berglund, Polymer **43**, 2445 (2002)
72. L.M. Guerrini, M.C. Branciforti, T. Canova, R.E.S. Bretas, Mater. Res.-Ibero-Am. J. **12**, 181 (2009)
73. H.R. Pant, M.P. Bajgai, C. Yi, R. Nirmala, K.T. Nam, W.-I. Baek, H.Y. Kim, Colloid Surface A **370**, 87 (2010)
74. X.S. Zhang, A. Gohn, G. Mendis, J.F. Buzinkai, S.J. Weigand, A.M. Rhoades, Macromolecules **54**, 7512 (2021)
75. F.Z. Rafique, N. Vasanthan, J. Phys. Chem. B **118**, 9486 (2014)
76. Q. He, Z. Wang, Y. Wang, Z. Wang, C. Li, R. Annapooranan, J. Zeng, R. Chen, S. Cai, Sci. Robot. **6**(57), 9704 (2021)
77. N. Vasanthan, D. Salem, J. Polym. Sci. B **39**, 536 (2001)
78. J. Li, L. Tian, N. Pan, Z.-J. Pan, Polym. Eng. Sci. **54**, 1618 (2014)
79. V. Krasinskyi, O. Suberlyak, J. Sikora, V. Zemke, Polym.-Plast. Technol. Mater. **60**, 1641 (2021)
80. J. Maillo, P. Pages, E. Vallejo, T. Lacorte, J. Gacen, Eur. Polym. J. **41**, 753 (2005)
81. S. Ali, A. Khatri, A. Javeed, S.H. Kim, J. Text. Inst. **111**, 723 (2020)
82. Z. Khatri, R.A. Arain, A.W. Jatoi, G. Mayakrishnan, K. Wei, I.S. Kim, Cellulose **20**, 1469 (2013)
83. Z. Khatri, A. Khatri, U. Saleem, G. Mayakrishnan, B.S. Kim, K. Wei, I.S. Kim, Color. Technol. **129**, 159 (2013)
84. T.N.T. Kim, K. Vu Thi Hong, N. Vu Thi, H. Vu Manh, Polymers **13**, 1434 (2021)
85. F. Taher, Aust. J. Basic Appl. Sci. **6**, 596 (2012)
86. F.K. Mahar, M. Mehdi, U.A. Qureshi, K.M. Brohi, B. Zahid, F. Ahmed, Z. Khatri, J. Mol. Liq. **248**, 911 (2017)
87. M. Khatri, F. Ahmed, A.W. Jatoi, R.B. Mahar, Z. Khatri, I.S. Kim, Ultrason. Sonochem. **31**, 350 (2016)
88. A. Abbasi, M.M. Nasef, M. Takeshi, R. Faridi-Majidi, Chin. J. Polym. Sci. **32**, 793 (2014)